Bias selectable dual band AlGaN ultra-violet detectors

Feng Yan[a], Laddawan Miko, David Franz, Bing Guan[a], Carl M. Stahle

NASA/Goddard Space Flight Center, Detector Systems Branch, Code 553,

Greenbelt, MD 20771

Bias selectable dual band AlGaN ultra-violet (UV) detectors, which can separate UV-A and UV-B using one detector in the same pixel by bias switching, have been designed, fabricated and characterized. A two-terminal *n-p-n* photo-transistor-like structure was used. When a forward bias is applied between the top electrode and the bottom electrode, the detectors can successfully detect UV-A and reject UV-B. Under reverse bias, they can detect UV-B and reject UV-A. The proof of concept design shows that it is feasible to fabricate high performance dual-band UV detectors based on the current AlGaN material growth and fabrication technologies.

---

[a] Feng Yan and Bing Guan work for NASA/Goddard through a contract between NASA/Goddard and MEI Technologies, Inc.

Ultra-violet (UV) detectors are of great importance for remote sensing, UV dose monitoring, dermatology and many other applications.[1,2,3,4] The UV spectrum is commonly classified into three regions, UV-A (315 nm to 400 nm), UV-B (280 nm to 315 nm) and UV-C (<280 nm). The atmospheric transmission efficiency drops drastically from UV-A to UV-C. UV-C photons are completely absorbed by the atmospheric ozone layer. The influence on lives and plants on the earth, especially on human beings, varies significantly from UV-A to UV-C. Thus, a multi-band UV detector and imaging technology, which can detect and image multiple UV bands, would be highly valuable.

AlGaN UV detectors and imaging technologies have been developed for many years.[5,6,7,8] One of the unique advantages of AlGaN wide bandgap semiconductors is that hetero-structures can be fabricated by tuning the ratio of Al in AlGaN. As a result, an intrinsic band-pass filter can be formed using AlGaN *p-i-n* hetero-structures with appropriate Al ratio in different layers, which can eliminate the need for the external blocking filters in many applications.[3,4] Also, the availability of AlGaN hetero-structures makes it feasible to fabricate multi-color UV detectors by stacking multiple junctions.

One technique for dual band detection is stacking two *p-n* structures back to back and forming a two terminal *n-p-n* photo-transistor-like structure.[9] However, different from photo-transistors, dual band detectors should be optimized for unity gain and the absorption in the center *p* region should be minimized. When a positive bias is applied between the top and bottom *n* layer, the top *n-p* junction is reversely biased, acting as a detector, and the bottom *p-n* junction is at forward bias, acting as a variable resistor. When the bias is flipped, the top *n-p* becomes a variable resistor and the bottom *p-n* junction becomes a detector. If the top and bottom detectors are designed to respond to

different spectra, two different bands can be sensed by switching the bias across the detector. This technology has been successfully used in a HgCdTe imaging IR detector.[5,10] In this paper, we present a novel AlGaN UV detector with a *n-p-n* hetero-structure, which can respond to UV-A and UV-B separately in the same pixel by switching the bias across the device.

An *n-p-n* multi-layer AlGaN structure has been designed for UV-A and UV-B detection based on the energy bandgap equation given by Yun,[11]

$$E_g(x) = E_{g1} \cdot x + E_{g0} \cdot (1-x) - b \cdot x \cdot (1-x), \quad (1)$$

where x is the ratio of Al, E_{g0} and E_{g1} are the energy bandgap for GaN (3.42eV) at room temperature and AlN (6.2eV) and the bowing factor, b, is 1.0eV. In the *n-p-n* dual band detector, there are five distinct layers, which are the n^+ for top ohmic contact layer, the first absorber doped with n^- or p^- , the center p^+ layer, the second n^- or p^- absorber, and the n^+ for bottom ohmic contact. Since the unintentionally doping for AlGaN is n type and the minimum doping concentration of n^- layers can be controlled to be lower than that of p^- layer, n^- doping is preferred for the two absorber layers.

Fig. 1 shows the SIMS doping concentration profiles of Si, Mg and Al ratio of the reference wafer, which has been grown and activated at the same conditions as the actual wafer used for detector fabrication. The five layers, labeled out as I, II, III, IV and V in Fig. 1, are Si-doped n^+ layer, Mg-doped p layer, Mg doped p^+ layer, Mg-doped p layer and Si doped n^+ layer from the surface to the bottom. The thicknesses of these five layers are 0.05μm, 0.3μm, 0.1μm, 0.3μm and 1μm, respectively. During the growth, the top GaN absorber (Layer II) was grown right after the growth of p^+ layer, which makes it p type due to the Mg memory effect.[12] The Mg concentration in the bottom n^- $Al_{0.2}Ga_{0.8}N$

layer (Layer IV) is also substantially higher than Si concentration, which is likely due to the out-diffusion of Mg during growth and activation annealing. The actual doping level for these two layers should be significantly lower than the Mg concentration shown in Fig. 1 but was not calibrated in our study. The variance of the type of the doping in the two absorbers, however, will only change the placement of the junctions. It will not affect the way to operate the detector since the direction of the top and bottom *p-n* junctions will not change.

It should also be noted that the Mg concentration due to the memory effect is very high in Layer II. Assuming a 10% activation efficiency of Mg, the doping concentration in this layer would be around $10^{17}/cm^3$. Thus the top junction becomes a n^+-p^+ junction. As a result, the depletion width in GaN absorber is smaller than that in $Al_{0.2}Ga_{0.8}N$ (Layer IV) for the same bias level.

The *n-p-n* detectors were defined by a mesa formed by conventional RIE etching. Ohmic contacts were formed by rapid thermal annealing of Ni-Au bi-layer deposited on the top and bottom *n* layer. Fig. 2 shows the cross-sectional view of the detectors and the inset shows the top view of a fabricated 300 μm diameter *n-p-n* dual band AlGaN detector. A and B are the electrodes on the bottom and top.

Fig. 3 shows the I-V characteristics measured with and without UV illumination using a Keithley 4200 semiconductor parameter analyzer. In the measurement, Electrode A, connecting to the bottom n^+ layer, is grounded and the bias on the electrode B on the top is scanned from -10 V to +10 V. The bottom I-V curve is measured in the dark. It is seen that the leakage current is lower than 10^{-12} A between -10 V and 5 V. The detectors become very leaky at biases above 5V and the leakage current increases rapidly from 5V

to 10V. The rapid increase is attributed to the poor junction quality of the top n^+-p^+ junction formed by the memory effect of Mg.

Under 290 nm back illumination, the photo-current is around 10^{-12} A under forward biases. Under reverse bias, the photo-current increases from 0.7 pA to 400 pA from 1 V to -1 V. From -1 V to -10 V, the photo-current increases slowly from 400 pA to 3 nA. Under 340 nm UV illumination, the photo-current is around 2 pA under reverse bias conditions. From -1 V to 1 V, it rapidly increases from 0.5 pA to more than 0.2 nA and then increases to 6 nA at 10 V. As shown in Fig. 3, under reverse bias, the detector is active for 290nm and blind to 340nm. The ratio of the photo-response at 290 nm and 340 nm is over two orders of magnitude under reverse bias. Under the forward bias, the detector is active to 340nm and blind to 290nm. The ratio of the photo-response at 340 nm and 290 nm is over three orders of magnitude under forward bias, indicating an excellent out-of-band rejection.

The external quantum efficiency was determined by comparing the photo-current vs. the incident power measured by Newport 1830-C power-meter with a calibrated Si photodiode. Fig. 4 shows the spectral quantum efficiency of a dual band UV detector with +5 V and -5 V applied on the top and the bottom being grounded. As shown in the figure, the detector at -5 V has the cut-on and cut-off wavelength at 280 nm and 315 nm, respectively. The cut-on wavelength corresponds to the bandgap of the $Al_{0.2}Ga_{0.8}N$ absorber (layer IV) and the cut-off wavelength corresponds to the bandgap of the $Al_{0.47}Ga_{0.53}N$ (Layer V). At +5 V, the cut-on and cut-off wavelength of the response spectrum are 320nm and 360nm, determined by the bandgap of $Al_{0.2}Ga_{0.8}N$ (Layer III and IV) and the top GaN absorber (Layer II). The peak quantum efficiency at +5 V and -5 V

is 14% and 25%, respectively. At -10 V, the peak quantum efficiency is over 65%. At +10 V, the peak quantum efficiency is 23%. Since the leakage current becomes very high at +10 V, the photo-current cannot be determined accurately and the photo-response spectrum is not shown in this figure. Both response spectra show clear cut-off and cut-on wavelength. The out-of-band rejection is over two orders of magnitude.

It is noted that the maximum quantum efficiency under forward bias is substantially lower than that under reverse bias. This can be explained by the difference of the doping levels for the two absorber layers. Due to the Mg memory effect, the doping level in GaN absorber (Layer II) is much higher than that in $Al_{0.2}Ga_{0.8}N$ (Layer IV). The depletion width in GaN absorber is smaller than that in $Al_{0.2}Ga_{0.8}N$ under the same bias level. Consequently, the quantum efficiency under forward biasing is lower than that under reverse biasing. The asymmetric response spectra for UV-A and UV-B can be eliminated by suppressing the Mg memory effect during the material growth. The maximum quantum efficiency for UV-A can be significantly improved.

One of the advantages of the *n-p-n* type photo-detectors is its compatibility with most standard readout electronics designed for regular photodiodes. Two different UV bands can be monitored using one pixel and the readout electronics developed for single band UV detectors. A large format photodiode array can be developed using standard Si readout chips commercially available for photodiode arrays. The development of a dual band UV AlGaN detectors has the advantage of sensing of two UV bands without sacrificing the optical resolution and introducing alias for UV multi-band imaging.

However, since the structure contains two back-to-back *p-n* junctions, the linearity may become an issue. As the photo-current increases, the voltage across the forward biased

junction has to increase and the voltage across the reverse biased junction is therefore reduced. As a result, the depletion width decreases and the quantum efficiency drops. For the structure we have investigated, the photocurrent continued to increase as the bias increased, indicating that the absorber is not fully depleted even for a -10 V bias. The linearity may not be good when the photo-current is high but needs to be investigated further. This problem may be solved by controlling the Mg memory effect and the out-diffusion of Mg to make the doping of the n^- GaN and $Al_{0.2}Ga_{0.8}N$ absorbers low enough so that they are fully depleted at the operating bias voltage level.

It should be pointed out that the same *n-p-n* structure can be designed to respond to two consecutive UV bands between 250nm and 365nm based on the current AlGaN growth technology. If the Al ratio in the center p^+ layer (Layer III) is different from Al ratio in the bottom absorber (Layer IV), the structure can be designed to respond to two different UV bands with the center wavelengths and the spectral resolution designable. The spectral resolution is only limited by the uniformity of the Al concentration.

In summary, an AlGaN dual band *n-p-n* photo-detector has been developed. Under forward bias condition, the detector can selectively sense UV photons between 320 nm and 365 nm. The maximum quantum efficiency at 10 V is 23%. Under reverse bias condition, the detector responds to UV photons between 280 nm and 315 nm. The maximum quantum efficiency at 10 V is over 65%. The low quantum efficiency in UV-A is caused by the poor junction quality of the top p^+-n^+ junction formed due to the Mg memory effect. It can be significantly improved by suppressing the Mg memory effect during the material growth.

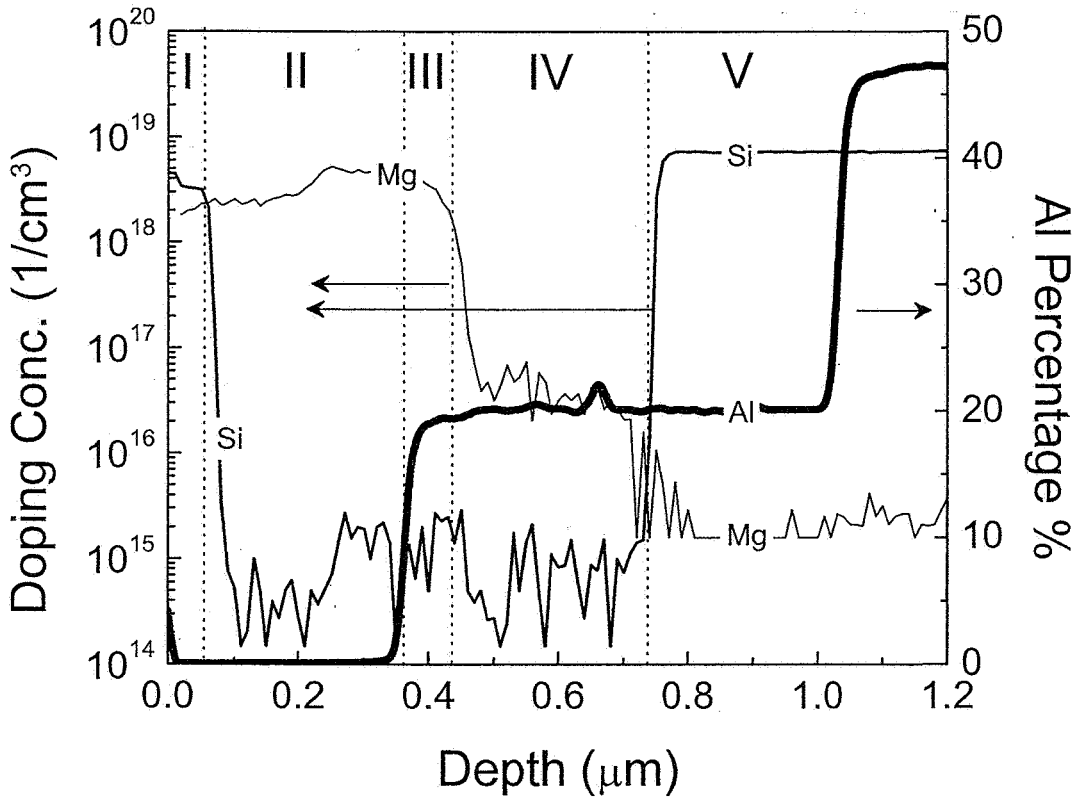

Figure 1. The SIMS profile of Mg, Si doping concentration (left axis) and Al ratio (right axis) of the starting wafer. The five function layers are separated by vertical dash lines and labeled on the top

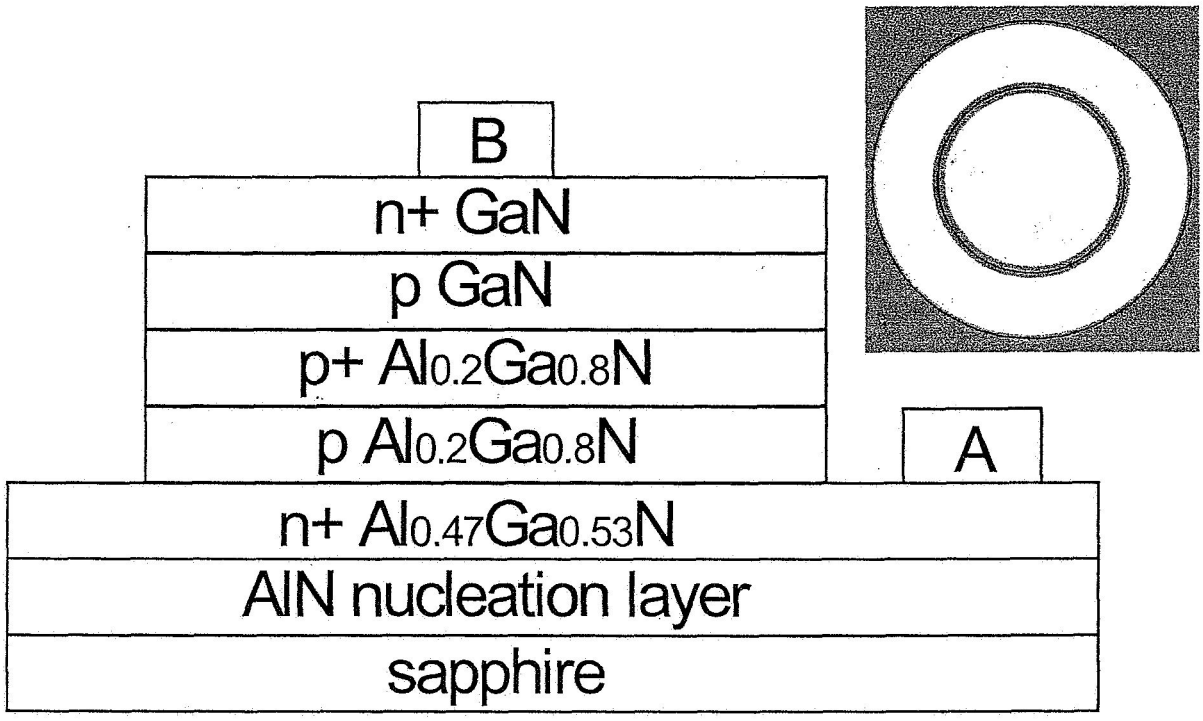

Figure 2. The cross-sectional view n-p-n dual band UV-A and UV-B detectors. The inset is a the top view picture of a 300um detector. A and B are the top and bottom electrodes.

[1] C. N. Hsu, J. R. Herman, J. F. Gleason, O. Torres, and C. J. Seftor, Geophy. Res. Lett. **26**, 1165 (1999).

[2] A. Richards, *Alien Vision: exploring the electromagnetic spectrum with imaging* (SPIE Press, Washington, 2001), Chap. 1.

[3] B. L. Diffey, Phys. Med. Biol. **36**, 299 (1991).

[4] B. A. K. Høiskar, R. Haugen, T. Danielsen, A. Kylling, K. Edvardsen, A. Dahlback, B. Johnsen, M. Blumthaler, and J. Schreder, Appl. Optics **42**, 3472 (2003).

[5] Y. Morimoto and S. Ushio, Jpn. J. Appl. Phys. **13**, 365 (1974).

[6] M. A. Khan, J. N. Kuznia, D. T. Olson, M. Blasingame, and A. R. Bhattarrai, Appl. Phys. Lett. **63**, 2455 (1993).

[7] J. P. Long, S. Varadaraajan, J. Mathews, and J. F. Schetzina, Opto-electronics Review **10**, 251 (2002).

[8] P. Lamarre, A. Hairston, S. P. Tobin, K. K. Wong, A. K. Sood, M. B. Reine, M. Pophristic, R. Brikham, I. T. Ferguson, R. Singh, C. R. Eddy, Jr., U. Chowdhury, M. M. Wong, R. D. Dupiuis, P. K. Kozodoy, and E. J. Tarsa, phys. stat. sol. **188**, 289 (2001).

[9] E. R. Blazejewski, J. M. Arias, G. M. Williams, W. Mclevige, and M. Zandian, J. Vac. Sci. Technol. B **10**, 1627 (1992).

[10] E. P. Smith, L. T. Pham, G. M. Venzor, E. Norton, M. Newton, P. Goetz, V. Randall, G. Pierce, E. A. Patten, R. A. Coussa, K. Kosai, W. A. Radford, J. Edwards, S. M. Johnson, S. T. Baur, J. A. Roth, B. Nosho, J. E. Jensen, and R. E. Longshore, Proc. of SPIE **5209**, 1 (2003).

[11] F. Yun, M. A. Reshchikov, L. He, T. King, H. Morkoc, S. W. Novak, and L. Wei, J. Appl. Phys. **92**, 4837 (2002).

[12] H. Xing, D. S. Green, H. J. Yu, T. Mates, P. Kozodoy, S. Keller, S. P. Denbaars, and U. K. Mishra, Jpn. J. Appl. Phys., Part I **42**, 50 (2003).